PAPER

Check for updates

Optimization of structural and electronic properties in CuO/CIGS hybrid solar cells for high-efficiency, sustainable energy conversion

Abdelghani Rahal,[ab] Idris Bouchama,[ab] M. A. Ghebouli,[ac] B. Ghebouli,[d] M. Fatmi, [ID] *[a] S. Alomairy,[e] S. Boudour,[f] F. Benlakhdar [ID] [f] and M. Chellouche[g]

This study presents a comprehensive analysis of the performance of hybrid solar cells based on copper oxide (CuO) and copper indium gallium selenide (CIGS) using the Solar Cell Capacitance Simulator-1D (SCAPS-1D) simulation software. The effects of copper oxide absorber layer thickness, acceptor density in the copper oxide and copper indium gallium selenide layers, and defect density on solar cell performance parameters, including conversion efficiency, open-circuit voltage, short-circuit current density, and fill factor, were analyzed. Results showed that the copper oxide/copper indium gallium selenide hybrid structure achieves enhanced conversion efficiency compared to the single copper oxide structure, with optimal values determined for absorber layer thickness, acceptor density, and defect density. This study provides valuable insights for developing high-efficiency, low-cost hybrid solar cells using abundant and non-toxic materials.

1. Introduction

The global pursuit of clean, renewable energy has driven substantial interest in hybrid solar cells that offer a promising balance between cost-effectiveness and high performance. Among the wide range of materials explored, copper oxide (CuO) has emerged as a potential p-type semiconductor owing to its narrow bandgap, high optical absorption coefficient, low cost, non-toxicity, and earth abundance. Integration of CuO nanoparticles into bulk-heterojunction (BHJ) devices has led to significant improvements in power conversion efficiency (PCE)—from 2.85% to 3.82%—mainly by enhancing visible light absorption and promoting charge separation due to the nanostructured surface morphology.[1] Numerical simulations using SCAPS-1D have indicated that CuO-based p–n junctions, particularly n-TiO$_2$/p-CuO cells, can theoretically achieve efficiencies as high as 22.4%, depending on temperature, work function, and interfacial defect density.[2] Despite challenges like non-uniform distribution and poor crystallinity in certain configurations, CuO consistently demonstrates strong light absorption across 400–800 nm, which validates its role as a light-absorbing layer in photovoltaic applications.[3] Vertically aligned CuO nanorod arrays grown at room temperature showed promising results as cathode materials in dye-sensitized solar cells (DSSCs), reaching efficiencies up to 0.29% while presenting an inexpensive alternative to platinum electrodes.[4] Hybrid composites of CuO with conducting polymers such as polyaniline (PANI) have improved thermal stability, electrical conductivity, and suitable band alignment, making them viable for integration into ITO/PANI-CuO/PCBM/Al structures.[5] Incorporating CuO nanoparticles as sensitizers in TiO$_2$-based solar cells has expanded light absorption to the visible region and enhanced charge carrier separation, supported by their narrow bandgap of ~1.2 eV.[6] Furthermore, depositing CuO nanoleaves onto monocrystalline silicon substrates significantly reduced reflectivity and increased effective light trapping in the 250–1250 nm range, boosting the overall device efficiency by 17.9%.[7] Theoretical models have also shown that tandem cells comprising CuO in conjunction with materials like ZnSnN$_2$ and GaInP can exceed 31% efficiency, highlighting the potential of CuO in multi-junction architectures when material properties are carefully optimized.[8] Additionally, doping CuO nanotubes with Fe enhanced crystallinity and reduced deep-level defects, although excessive doping caused reduced surface area and charge mobility, leading to diminished performance.[9] In inverted hybrid devices containing a ternary active layer of CuO/P3HT/PCBM, the inclusion of

[a] *Research Unit on Emerging Materials (RUEM), University Ferhat Abbas, Setif, Algeria. E-mail: fatmimessaoud@yahoo.fr*

[b] *Department of Electronics, Faculty of Technology, University of M'sila, M'sila, 28000, Algeria*

[c] *Department of Chemistry, Faculty of Sciences, University of M'sila University Pole, Road Bourdj Bou Arreiridj, M'sila, 28000, Algeria*

[d] *Laboratory for the Study of Surfaces and Interfaces of Solid Materials (LESIMS), University Ferhat Abbas of Setif 1, Setif, 19000, Algeria*

[e] *Department of Physics, College of Science, Taif University, Taif 21944, Saudi Arabia*

[f] *Research Center in Industrial Technologies CRTI, P.O. Box 64, Cheraga, Algiers 16014, Algeria*

[g] *Faculty of Exact Sciences, Environmental Engineering Laboratory, University of Béjaïa, Béjaïa, 06000, Algeria*

CuO improved open-circuit voltage, crystallinity, and current density, increasing efficiency from 3.4% to 3.7%.[10] Similarly, Mn-doped CuO nanowires enhanced visible light absorption and charge separation, with 2% Mn yielding optimal efficiency, while higher doping levels degraded the structure and performance.[11] Simulations on ZnO/CuO/Cu₂O heterojunctions demonstrated that precise tuning of thickness and doping concentration could achieve efficiencies up to 12.18%.[12] CuO was also proven to be an effective bandgap-reducing agent in PANI-CuO-PCBM hybrid solar cells, leading to a PCE of 1.31%.[13] A two-step sputtering process in p-CuO/n-Si heterojunction cells helped minimize the Cu-rich interfacial layer and improved crystallinity, resulting in a record efficiency of 1.21% for that structure.[14] Low-concentration doping of CuO with Fe and Mn nanoparticles (2%) further improved charge separation and enhanced PCE from 0.50% to 0.84%, whereas higher dopant levels introduced recombination centers and impaired conductivity.[15] Moreover, SCAPS-based simulations of CuO/TiO₂ heterojunctions revealed that maximum efficiencies (~23%) could be achieved with a CuO thickness of 4.0 μm and TiO₂ thickness of 0.3 μm, provided that defect densities—especially in the CuO layer—are minimized.[16] Nanoflake-shaped CuO structures synthesized *via* a wet-chemical method displayed a pure monoclinic phase, low-defect density, and a bandgap of 1.45 eV, making them suitable candidates as absorbing layers in solar cells.[17] CuO nanoparticles blended into P3HT/PC₇₀BM matrices boosted device efficiency by 40.7%, mainly through improved crystallinity, enhanced light scattering, and reduced recombination at the donor–acceptor interface.[18] Finally, CuO nanocoatings fabricated *via* chemical oxidation showed high solar absorptance (~92%) and low thermal emittance (~13%), underlining their potential as selective solar absorbers for photothermal energy harvesting.[19]

2. Modeling and simulation

2.1. Solar cell structure

In this study, we simulated two types of solar cell structures: CuO-based solar cell with a structure of FTO/ZnO/CdS/CuO/Au and CuO/CIGS hybrid solar cell with a structure of FTO/ZnO/CdS/CuO/CIGS/Au, as shown in Fig. 1. In both structures, the FTO (fluorine-doped tin oxide) layer serves as a transparent front electrode, the ZnO layer serves as a front window, the CdS layer serves as a buffer layer, the CuO layer serves as a main absorber layer, and Au serves as a back electrode. In the hybrid structure, a CIGS layer was added between CuO and the back electrode to enhance light absorption and charge separation.

2.2. Simulation model

SCAPS-1D software (version 3.3.07) was used to simulate the performance of the solar cells. The program solves the Poisson and continuity equations for charge carriers (electrons and holes) to determine the current–voltage (*J*–*V*) characteristics and quantum efficiency (QE) of the solar cell under standard AM1.5G illumination conditions (100 mW cm⁻²) and a temperature of 300 K. The input parameters used in the simulation are derived from the literature and are shown in Table 1. These parameters include the physical and electrical properties of each layer, such as layer thickness, bandgap, electron affinity, relative permittivity, carrier density, mobility, density of states in conduction and valence bands, thermal velocity, and electron and hole capture cross-sections.

2.3. Optimization studies

To determine the optimal conditions for achieving maximum cell efficiency, we conducted systematic studies of the effect of the following parameters:

1. CuO absorber layer thickness (ranging from 0.1 to 5.0 μm)
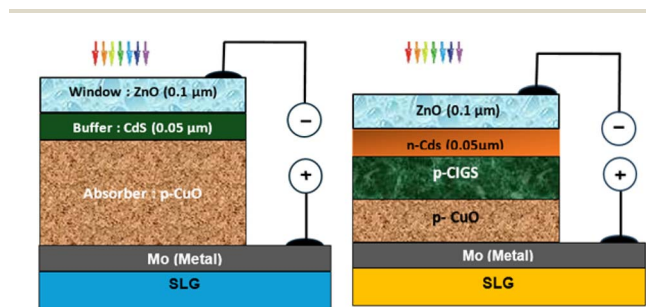2. Acceptor density in the CuO layer (ranging from 10^{15} to 10^{19} cm⁻³)

Fig. 1 Block diagram of CuO/CdS/ZnO and CuO/CIGS solar cell structures.

Table 1 Input parameters used in SCAPS-1D simulator

	CuO	CIGS	Co₂O	CdS	ZnO
Thickness (μm)	3	Varied	3	0.1	0.08
Band gap (eV)	1.51	1.2	2.17	2.4	3.3
Electron affinity (eV)	4.07	4.5	3.20	4.2	4.6
Dielectric permittivity (relative)	18.10	10	7.11	10	9
CB (conduction band) effective density of states (cm³)	2.2×10^{19}	2×10^{18}	2×10^{17}	1×10^{18}	2.2×10^{18}
VB (valence band) (cm⁻³)	5.5×10^{20}	2×10^{18}	1.1×10^{19}	1.5×10^{19}	1.8×10^{19}
Electron mobility μ_n (cm² V⁻¹ s⁻¹)	100	10	200	100	100
Hole mobility μ_p (cm² V⁻¹ s⁻¹)	0.1	2.5	80	25	25
Shallow uniform donor density N_D (cm⁻³)	0	0	0	1×10^{17}	1×10^{19}
Shallow uniform acceptor density N_A (cm⁻³)	1×10^{16}	Varied	1×10^{18}	0	0

3. Acceptor density in the CIGS layer (ranging from 10^{15} to 10^{19} cm^{-3})

4. Defect density in the CuO layer (ranging from 10^{13} to 10^{17} cm^{-3})

5. Defect density in the CIGS layer (ranging from 10^{13} to 10^{17} cm^{-3})

For each set of parameters, we calculated the main cell performance parameters: conversion efficiency (η), open-circuit voltage (V_{oc}), short-circuit current density (J_{sc}), and fill factor (FF). We also analyzed the quantum efficiency (QE) curves to understand the spectral response of the cells.

3. Results and discussion

3.1. Energy band diagram

Fig. 2 shows the energy band diagram of the CuO and CuO/CIGS solar cells. In the CuO structure, the interface between CdS (n-type) and CuO (p-type) forms a main p–n junction that separates and collects photogenerated charge carriers. In the CuO/CIGS hybrid structure, the energy band alignment between CuO and CIGS is favorable for hole transport, while the CdS/CuO interface separates electrons. This cascade configuration of
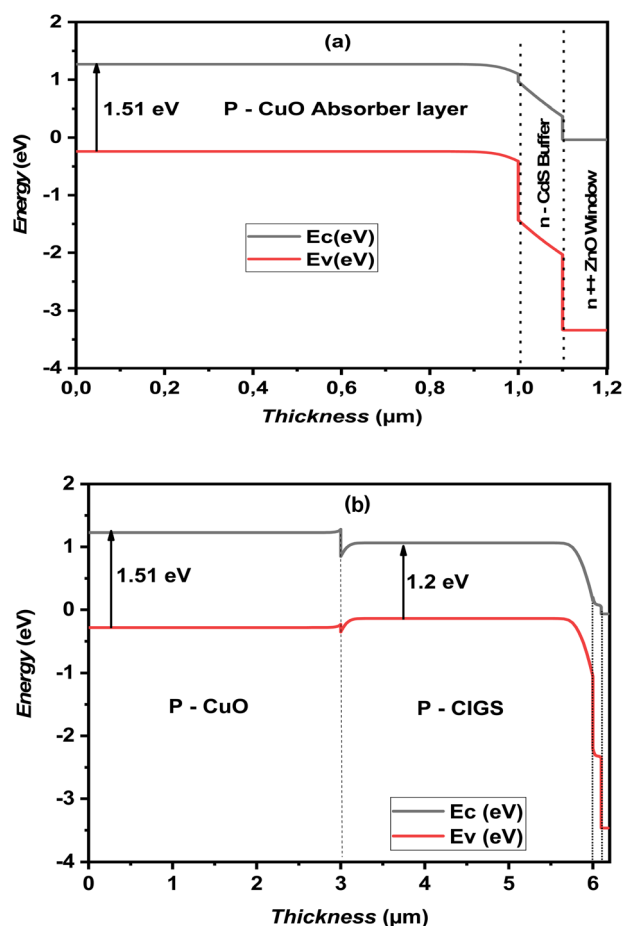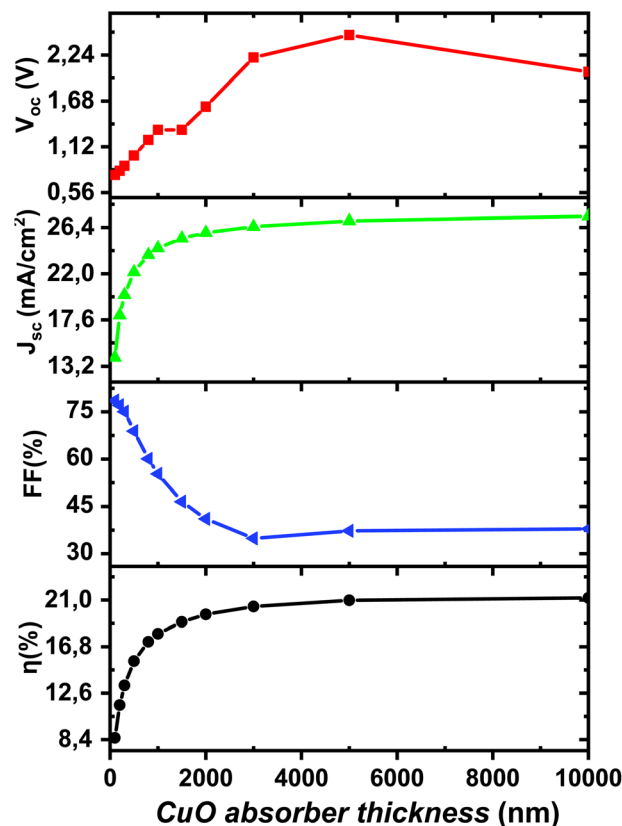

Fig. 3 Cell performance parameters as a function of CuO absorber layer thickness.

bands facilitates effective charge separation and reduces recombination, leading to improved cell performance.

3.2. Effect of CuO layer thickness

The effect of CuO absorber layer thickness on solar cell performance shows in Fig. 3. For the simple CuO cell, the conversion efficiency (η) increases with increasing CuO thickness until it reaches an optimal value at approximately 2.0 μm, then slightly decreases with further thickness increase. This behavior can be explained by the balance between light absorption and charge collection. As thickness increases, light absorption increases, leading to increased charge carrier generation and hence increased J_{sc}. However, with larger thicknesses, the diffusion distance of charge carriers to the electrodes becomes longer, increasing the probability of recombination and reducing charge collection efficiency. For the CuO/CIGS hybrid cell, we observe a similar trend, but with notably higher conversion efficiency across all CuO thicknesses studied. The maximum efficiency of the hybrid cell reaches approximately 18.5% at the optimal CuO thickness of 2.5 μm, compared to 12.7% for the simple CuO cell. V_{oc} shows weak dependence on CuO thickness in both structures, while J_{sc} increases significantly with increasing thickness until it reaches saturation.

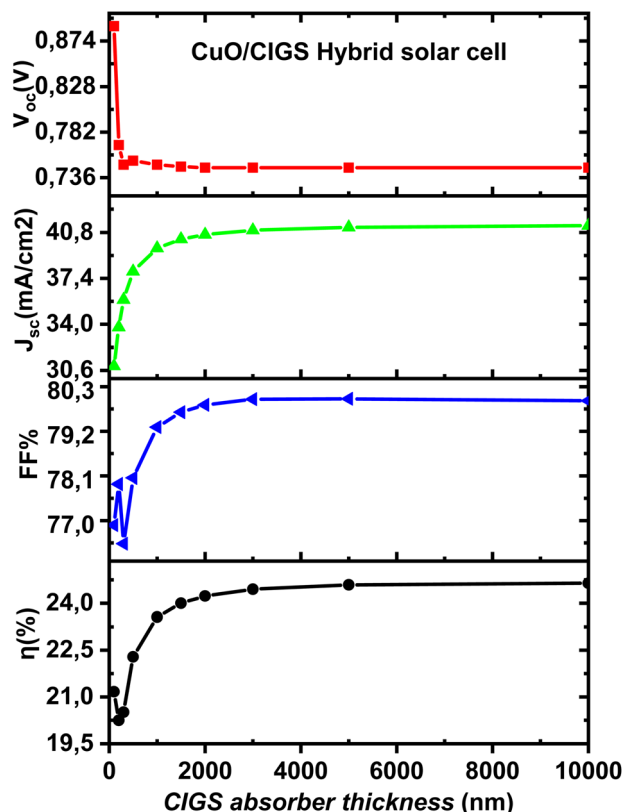Fig. 2 Band diagram for CuO and CuO/CIGS solar cells structures.

Fig. 4 Performance of CuO/CIGS hybrid solar cells depending on CIGS absorber layer thickness.

The fill factor (FF) remains relatively stable at lower thicknesses and then slightly decreases at larger thicknesses. Fig. 4 shows the effect of CIGS layer thickness on the performance of the CuO/CIGS hybrid cell. The conversion efficiency increases with increasing CIGS thickness up to about 1.5 μm, then stabilizes at a maximum value of approximately 19%. This indicates that the optimal CIGS thickness lies in the range of 1.5–2.0 μm, which is a reasonable value from both manufacturing and cost-effectiveness perspectives.

Mechanistically, the enhanced efficiency of the CuO/CIGS hybrid structure compared to a single CuO cell arises from the complementary optical and electronic properties of the two absorber layers. CuO, with its relatively large direct bandgap (∼1.5 eV), efficiently absorbs high-energy photons in the visible range (400–800 nm) but lacks absorption in the near-infrared region. CIGS, with a smaller bandgap (∼1.1 eV), compensates for this limitation by harvesting lower-energy photons (800–1200 nm) that pass through the CuO layer. This combination extends the spectral response and increases photogenerated current. In addition to spectral complementarily, the favorable band alignment between CuO and CIGS facilitates efficient charge separation and minimizes interfacial recombination, thereby enhancing the open-circuit voltage and fill factor. These synergistic effects contribute to the superior overall performance of the hybrid solar cell. However, this performance advantage comes with challenges. The integration of two

distinct semiconductor materials demands precise interface engineering, optimized deposition processes, and careful control of defects to maintain proper band alignment. Moreover, CIGS relies on relatively scarce and costly elements such as indium and gallium, whereas single CuO cells benefit from abundant, low-cost materials and simpler device structures. Despite the increased complexity and potential cost implications, the substantial gains in conversion efficiency may justify the hybrid approach, especially when assessed in terms of cost per watt rather than cost per unit area. Addressing these fabrication and material challenges is essential for evaluating the commercial viability of CuO/CIGS hybrid solar cells and guiding future technological advancements. To benchmark the performance of the proposed CuO/CIGS hybrid solar cell, which achieved a conversion efficiency of approximately 19%, we compare it with recently reported solar cell architectures simulated using SCAPS-1D. A notable example is the ZrS_2/CuO heterojunction, which demonstrated an efficiency of 23.8% due to its favorable band alignment and reduced defect density.[20] Similarly, a $BaZrS_3$/CuO hybrid structure exhibited a remarkable efficiency of 27.3%, benefiting from strong light absorption and optimal band offset between layers.[21] These comparisons indicate that the CuO/CIGS hybrid structure offers a balanced approach, combining respectable efficiency with relatively simple fabrication and the use of non-toxic, earth-abundant materials. Its improved spectral response, driven by the tandem bandgap absorption of CuO (∼1.5 eV) and CIGS (∼1.1 eV), along with favorable charge separation, positions it as a promising alternative for scalable, sustainable photovoltaic technologies.

3.3. Quantum efficiency

The quantum efficiency (QE) curves for CuO and CuO/CIGS solar cells shows in Fig. 5. The simple CuO cell exhibits good spectral response in the wavelength range of 400–800 nm, with
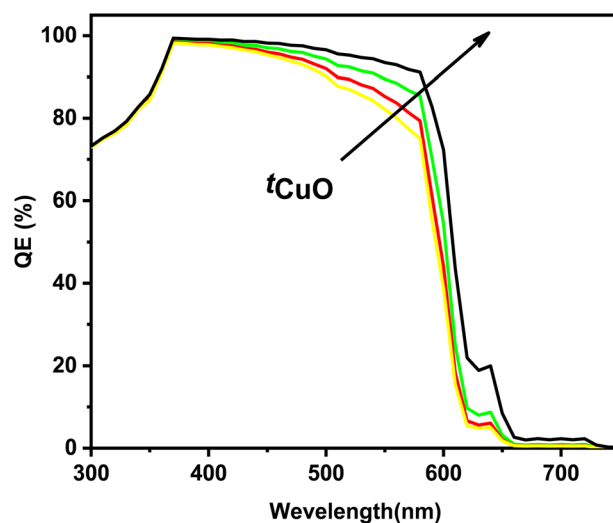

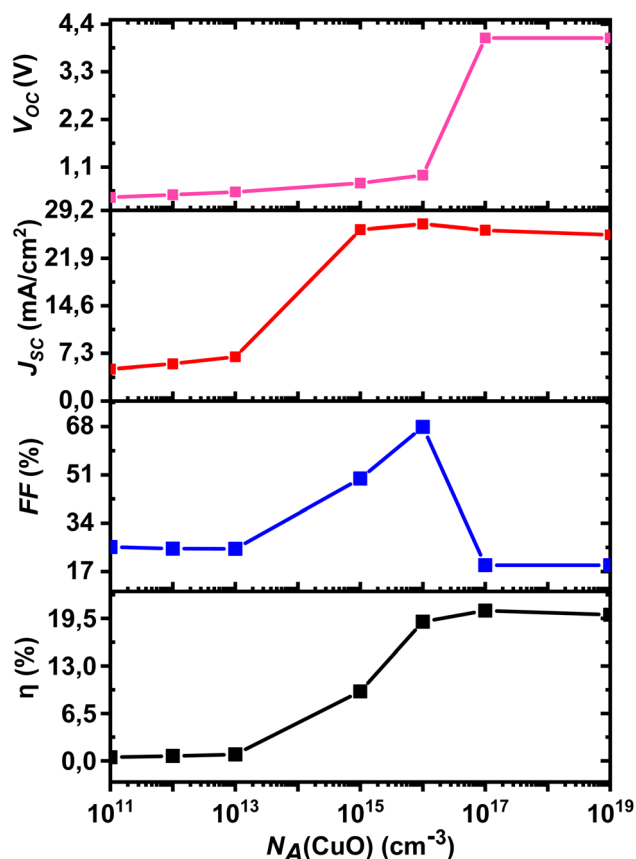Fig. 5 Quantum efficiency of CuO and CuO/CIGS solar cells structures.

Fig. 6 Impact of acceptor density of CuO absorber layer on cell performance.
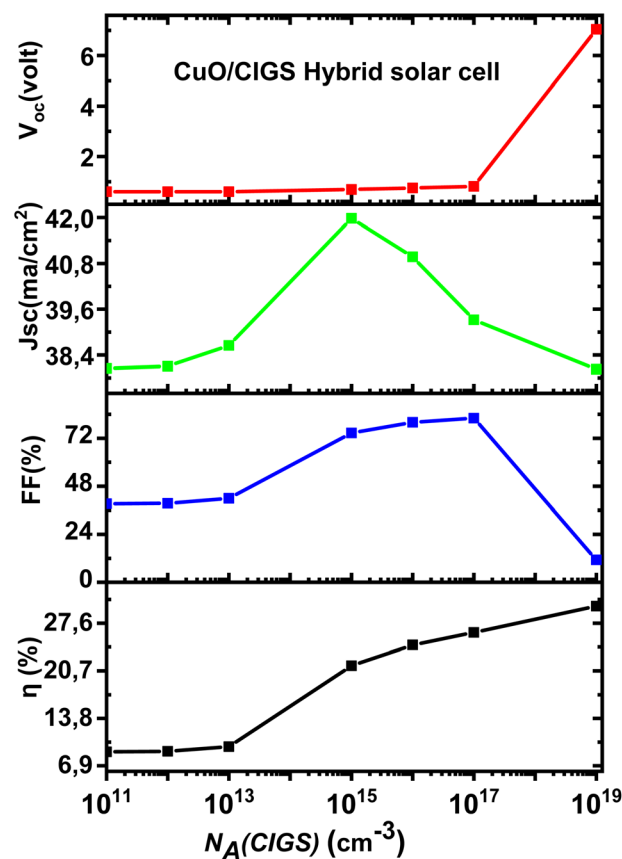

Fig. 7 Effect of acceptor density of CIGS layer on CuO/CIGS hybrid solar cell performance.

a decline in QE at longer wavelengths. On the other hand, the CuO/CIGS hybrid cell shows significant improvement in spectral response, especially in the longer wavelength range (800–1200 nm). This enhancement is due to the smaller bandgap of CIGS (about 1.1 eV) compared to CuO (about 1.5 eV), allowing for better absorption of lower-energy photons. As a result, the hybrid cell can utilize a broader range of the solar spectrum, leading to increased J_{sc} and η.

3.4. Effect of acceptor density

Fig. 6 shows the effect of acceptor density in the CuO layer on solar cell performance. For the simple CuO cell, the conversion efficiency increases with increasing acceptor density until it reaches an optimal value at approximately 10^{17} cm^{-3}, then drops sharply at higher densities. V_{oc} increases steadily with increasing acceptor density, due to increased band bending and improved charge separation. However, J_{sc} and FF decrease at very high acceptor densities, resulting in a decrease in overall efficiency. The CuO/CIGS hybrid structure shows a similar trend, with maximum conversion efficiency at a CuO acceptor density of approximately 5×10^{16} cm^{-3}. The decrease in efficiency at high acceptor densities can be attributed to increased Auger recombination and decreased minority carrier diffusion length.

The effect of CIGS acceptor density on the performance of the CuO/CIGS hybrid cell shows in Fig. 7. The efficiency increases with increasing CIGS acceptor density up to about 10^{16} cm^{-3}, then gradually decreases. This result is consistent with previous studies showing that the optimal acceptor density for CIGS solar cells lies in the range of 10^{15}–10^{17} cm^{-3}.
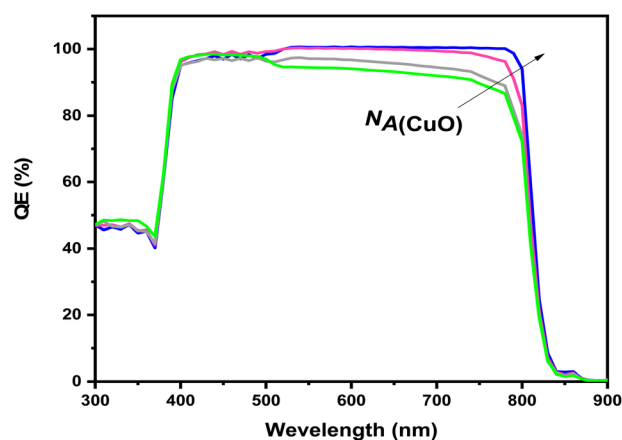

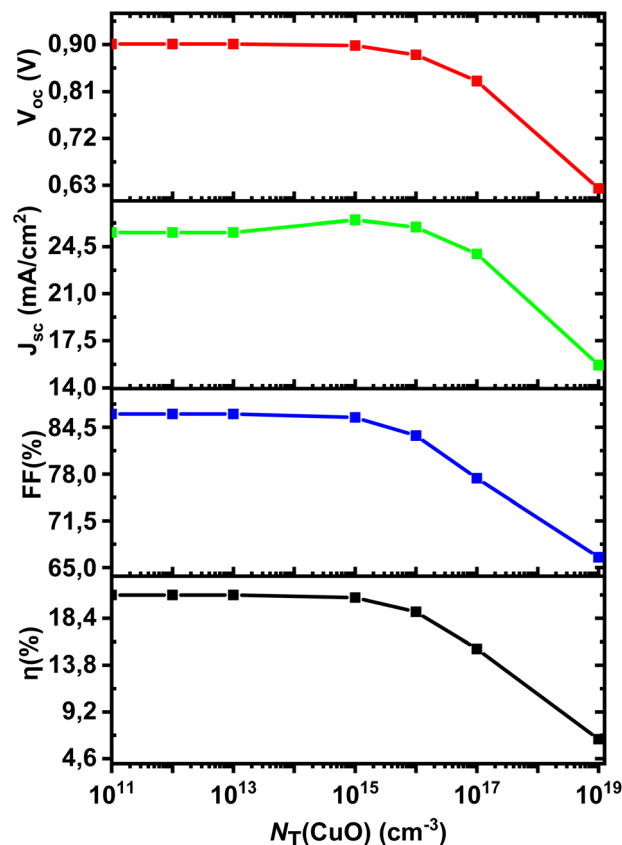**Fig. 8** Quantum efficiency QE of CuO solar cell for various acceptor concentrations.

Fig. 9 Variation of solar cell performance with varying of defect density of CuO absorber layer.
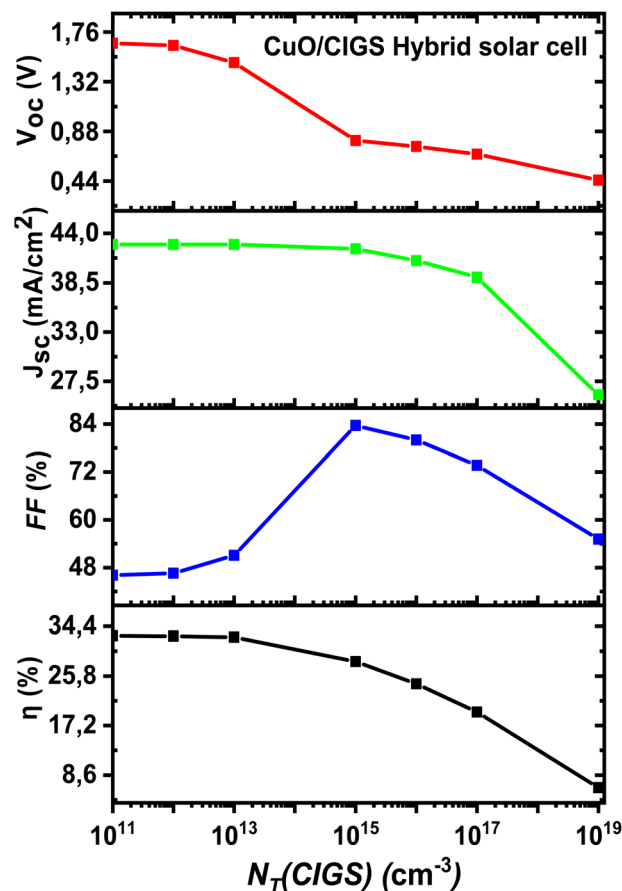

Fig. 10 Effect of defect density of CIGS layer on CuO/CIGS hybrid solar cell performance.

Fig. 8 shows the effect of acceptor density on the quantum efficiency (QE) curves of the CuO solar cell. As the acceptor density increases, the QE improves in the mid-wavelength range (500–700 nm), indicating improved charge separation and collection. However, at very high acceptor densities (>10^{18} cm^{-3}), the QE decreases, especially at longer wavelengths, due to reduced minority carrier diffusion length.

3.5. Effect of defect density

Fig. 9 shows the effect of defect density in the CuO layer on solar cell performance. The conversion efficiency decreases significantly with increasing defect density, especially when it exceeds 10^{15} cm^{-3}. V_{oc}, J_{sc}, and FF decrease with increasing defect density, indicating increased recombination through defect centers. For high efficiency, it is essential to reduce the defect density in the CuO layer to below 10^{14} cm^{-3}. The CuO/CIGS hybrid structure shows better resistance to defect effects compared to the simple CuO cell. At similar defect density, the hybrid cell maintains higher conversion efficiency, suggesting that the presence of the CIGS layer can mitigate the negative effects of defects in the CuO layer. Fig. 10 shows the effect of CIGS defect density on the performance of the hybrid cell. As expected, the efficiency decreases with increasing defect density, but the decrease is less steep compared to the effect of

CuO defects. This indicates that the performance of the hybrid cell is more sensitive to the quality of the CuO layer compared to the CIGS layer. Fig. 11 shows the effect of CuO defect density on the quantum efficiency curves. As the defect density increases,
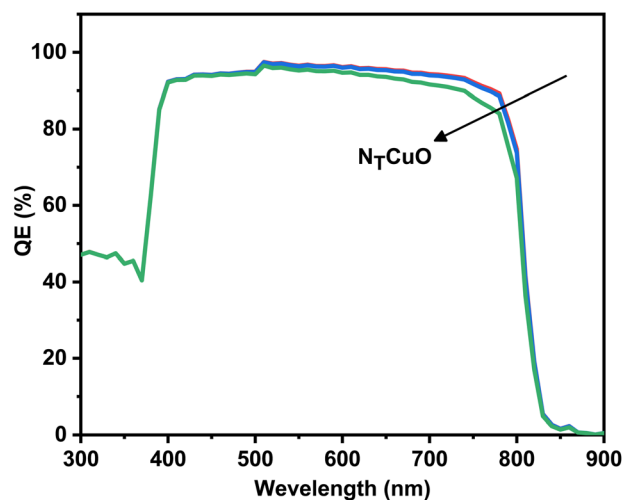

Fig. 11 Quantum efficiency *versus* wavelength of CuO solar cell with various N_T (CuO).

the QE decreases across the entire spectrum, with a more pronounced effect at longer wavelengths. This corresponds to a decrease in minority carrier diffusion length due to increased recombination.

4. Conclusion

In this study, we conducted a comprehensive analysis of the performance of CuO/CIGS hybrid solar cells using SCAPS-1D simulation. The effects of key parameters, including absorber layer thickness, acceptor density, and defect density, on cell performance parameters were systematically investigated. The results showed that the CuO/CIGS hybrid structure achieves significantly higher conversion efficiency compared to the single CuO structure, with a maximum efficiency of approximately 19% *versus* 12.7%. Our findings indicate that the optimal CuO layer thickness ranges between 2.0 and 2.5 μm, while the optimal CIGS thickness is approximately 1.5 μm. The optimal acceptor density for the CuO layer is around 5×10^{16} cm^{-3}, while the optimal acceptor density for the CIGS layer is around 10^{16} cm^{-3}.

For high efficiency, the defect density in both layers should be maintained below 10^{14} cm^{-3}. This efficiency threshold is directly linked to the mechanistic impact of defects on device performance. High defect densities introduce recombination centers within the absorber layers, significantly reducing the minority carrier lifetime and diffusion length. This limits the number of photogenerated carriers that successfully reach the junction and contribute to the photocurrent, thereby lowering the short-circuit current density and overall conversion efficiency. Moreover, defect states near the interface can create energy barriers that hinder efficient charge extraction and reduce the open-circuit voltage and fill factor. Therefore, controlling and minimizing defect densities is critical to achieving efficient carrier collection and maximizing the performance of CuO/CIGS hybrid solar cells. This study provides valuable guidance for designing and optimizing high-efficiency CuO/CIGS hybrid solar cells. Future work can extend this analysis to investigate additional factors such as temperature effects, interface composition, and alternative hybrid configurations, including CuO combined with emerging materials such as perovskites, to further improve device performance.

Data availability

Data underlying the results presented in this paper are not publicly available at this time but may be obtained from the corresponding author (fatmimessaud@yahoo.fr) upon reasonable request.

Conflicts of interest

The authors declare that they have no conflict of interest.

Acknowledgements

References

1 H. Siddiqui, *et al.*, Utility of copper oxide nanoparticles (CuO-NPs) as efficient electron donor material in bulk-heterojunction solar cells with enhanced power conversion efficiency, *J. Sci.:Adv. Mater. Devices*, 2020, **5**, 104–110.

2 P. Sawicka-Chudy, *et al.*, Simulation of TiO$_2$/CuO solar cells with SCAPS-1D software, *Mater. Res. Express*, 2019, **6**, 085918.

3 H. Kidowaki, *et al.*, Fabrication and characterization of CuO-based solar cells, *J. Mater. Sci. Res.*, 2012, **1**(1), 138–143.

4 S. Anandan, *et al.*, Room temperature growth of CuO nanorod arrays on copper and their application as a cathode in dye-sensitized solar cells, *Mater. Chem. Phys.*, 2005, **93**, 35–40.

5 S. Ashokan, *et al.*, Synthesis and characterization of CuO nanoparticles, DBSA doped PANI and PANI/DBSA/CuO hybrid composites, *J. Alloys Compd.*, 2015, **646**, 40–48.

6 N. Baranwal, *et al.*, Synthesis of CuO nanoparticles and their application as sensitizer in TiO$_2$ based solar cells, *J. Mater. Sci.: Mater. Electron.*, 2016, **27**, 3159–3165.

7 Y. Xia, *et al.*, CuO Nanoleaves Enhance c-Si Solar Cell Efficiency, *J. Mater. Chem. A*, 2013, **1–3**, 1–5.

8 T. Mohammed, *et al.*, Numerical study and design of tandem solar cells based on CuO as absorber layer using SCAPS, *RSC Adv.*, 2021, **11**, 20814–20823.

9 M. ul Haq, *et al.*, Effect of Fe doping on the crystallinity of CuO nanotubes and the efficiency of the hybrid solar cells, *J. Photochem. Photobiol., A*, 2017, **335**, 112–118.

10 M. Ikram, *et al.*, Efficient inverted hybrid solar cells using both CuO and P3HT as electron donor materials, *J. Mater. Sci.: Mater. Electron.*, 2015, **26**, 6478–6483.

11 M. Iqbal, *et al.*, Influence of Mn-doping on the photocatalytic and solar cell efficiency of CuO nanowires, *Inorg. Chem. Commun.*, 2017, **81**, 1–9.

12 N. D. Lam, Modelling and numerical analysis of ZnO/CuO/Cu$_2$O heterojunction solar cell using SCAPS, *Eng. Res. Express*, 2020, **2**, 025033.

13 R. Mahajan, *et al.*, Structural, optical, and electrical study of PANI-CuO-PCBM-based hybrid solar cell, *J. Mater. Sci.: Mater. Electron.*, 2019, **30**, 9354–9360.

14 S. Masudy-Panah, *et al.*, Reduction of Cu-rich interfacial layer and improvement of bulk CuO property through two-step sputtering for p-CuO/n-Si heterojunction solar cell, *J. Appl. Phys.*, 2014, **116**, 074501.

15 M. Iqbal, *et al.*, Synthesis and characterization of transition metals doped CuO nanostructure and their application in hybrid bulk heterojunction solar cells, *SN Appl. Sci.*, 2019, **1**, 647.

16 P. Sawicka-Chudy, *et al.*, Numerical analysis and optimization of Cu$_2$O/TiO$_2$, CuO/TiO$_2$ heterojunction solar cells using SCAPS, *J. Phys.: Conf. Ser.*, 2018, **1033**, 012002.

17 H. Siddiqui, *et al.*, Valuation of copper oxide (CuO) nanoflakes for its suitability as an absorbing material in solar cells fabrication, *Optik*, 2016, **127**(8), 3713–3717.

18 A. Wanninayake, *et al.*, CuO Nanoparticles Based Bulk Heterojunction Solar Cells: Investigations on Morphology and Performance, *J. Sol. Energy Eng.*, 2015, **137**(3), 031016.

19 G. G. Welegergs, *et al.*, Structural and optical properties of copper oxide (CuO) nanocoatings as selective solar absorber, *Mater. Today: Proc.*, 2021, **36**(2), 509–513.

20 M. Abdelfatah, A. M. El Sayed, W. Ismail, S. Ulrich, V. Sittinger and A. El-Shaer, SCAPS simulation of novel inorganic ZrS$_2$/CuO heterojunction solar cells achieving ~23.8% efficiency, *Sci. Rep.*, 2023, **13**, 4553.

21 A. A. El-Naggar, L. A. Lotfy, A. A. Felfela, W. Ismail, M. Abdelfatah, W. W. Sharshir and A. El-Shaer, Numerical simulation of an inorganic BaZrS$_3$/CuO heterojunction solar cell achieving 27.3% efficiency, *Sci. Rep.*, 2024, **14**, 7614.